

Short Communication

Electrochemical behaviour of API 5L X52 Steel Samples Immersed in Sulphate Aqueous Solutions with Different pH

Perla Morales Gil^{1,*}, Baptiste Julien², Manuel Palomar-Pardavé²,
María Guadalupe Montes de Oca-Yemha², María Teresa Ramírez-Silva³, Mario Romero-Romo^{2,*}

¹ Instituto Mexicano del Petróleo, Laboratorio de Caracterización de Materiales Sintéticos y Naturales, Eje Central Lázaro Cárdenas 152, Mexico City, CP 07730, CDMX, MÉXICO

² INSA - LYON - Domaine Scientifique de la Doua - 20, Rue Albert Einstein 69621 Villeurbanne Cedex – France.

³ Universidad Autónoma Metropolitana-Azcapotzalco, Departamento de Materiales, Av. San Pablo 180 Col. Reynosa-Tamaulipas, Mexico City, CP 02200, CDMX, MÉXICO.

⁴ Universidad Autónoma Metropolitana-Iztapalapa, Departamento de Química, Av. San Rafael Atlixco #186, Col. Vicentina, Mexico City, CP 09340, CDMX. MÉXICO.

*E-mail: moralesp@imp.mx (P.M.G) and mmrr@correo.azc.uam.mx (M.R.R.)

Received: 7 November 2017 / Accepted: 18 January 2018 / Published: 6 March 2018

Formation of anodic films was induced through application of potential pulses on the surface of API 5L X52 steel samples immersed in a 0.1 M H₂SO₄ aqueous solution with different pH set by adding NaOH. The formation mechanism was studied using the step potential technique to produce *j-t* plots, and the morphology and composition of the resulting films was characterized through SEM and EDX, respectively, and their passivating capacity was also electrochemically evaluated. It is shown that the anodic film was formed, in all cases, by means of nucleation and growth phenomena and that it cannot passivate the corrosion process. Furthermore, the nature of the films formed was also validated from a thermodynamic analysis based on the predominance zones diagram.

Keywords: Steel; Anodic films; pH; Potentiostatic current transients

1. INTRODUCTION

Pipelines built under the API 5L specification are designed and built for transportation of crude oil or for refined produce delivery. The mexican oil producing industrial group, PEMEX, formed by a group of enterprises developing a diversity of related businesses, operate and maintain an extensive underground and otherwise pipeline network, which normally conveys entrapped amounts of water-based fluids that can become the active electrolyte of corrosion microcells forming over the steel microstructure. Since the entrained waters largely contain a diversity of anions and other chemical

species that are basic to the spread, or contribute to arrest, internal corrosion phenomena through a diversity of chemical reactions. Looking over the possibility to arrest a significant problem that affects lastly the oil-based economy, and its fundamental infrastructure, Bruzzoni and Garavaglia [1] Have shown that anodic iron oxide film formed in 0.1 N NaOH may influence the formation and hydrogen transport properties and that the presence of hydrogen within the film causes a partial loss of the passivating properties of the film and an increase in the corrosion current. Hernández-Espejel *et al* [2] have characterized, using Scanning Electron Microscopy (SEM), X-ray Diffraction (XRD), Linear Polarization and Electrochemical Impedance Spectroscopy (EIS) techniques, the corrosion films formed, by voltammetry, on APIX52 pipeline steel in simulated acid sour media showed that the films are mainly composed of sulphide compounds (mackinawite, troilite, marcasite and pyrite) as well as iron oxides and from the potential step electrochemical technique [3] the kinetics and mechanism of the anodic film was determined. It was concluded that the electrochemical anodic film formation involves an E_1CE_2 mechanism, whereby the first of the two simultaneous processes were the Fe electrochemical oxidation (E_1) followed by FeS precipitation (C) that occurs by 3D nucleation and growth limited by mass transfer reaction and FeS oxidation (E_2) forming a mix of different stoichiometry iron sulphides and oxides. Therefore, this work deals in detail with the formation of surface sulphate-based anodic layers that can either give rise to passivity or conversely, to iron dissolution in sulphate media at different pH values, since this parameter is crucial for undertaking corrosion studies [4-7].

As reported by Rojas-Hernández *et al.* [8-11], the Predominance Zones Diagrams, PZD, facilitate analysis of the physico-chemical relevant features of the system under study, consider the concentration of some species and their associated reactions thermodynamic constants in aqueous solution [12] as a function of pH, within as wide a range as required. Such being the case, it is possible to note from Figure 1 that in an aqueous solution having an $[Fe(II)] 10^{-6}$ M, the formation of solid $Fe(OH)_2$ will predominate in the $9.45 \leq pH \leq 13.1$ range. Yet, at other pH values the reaction products formed due to interaction with the steel substrate will be expected to be soluble species namely Fe^{2+} or $FeSO_4$. Similarly, respect to the nature of the Fe(III) species formation, due also to oxidation of the substrate, it will depend on the pH as stated before. The insoluble species $Fe(OH)_{3(s)}$ or $Fe(OH)_{2(s)}$, can precipitate on a variety of sites upon reaching the appropriate concentration conditions, including defective or, simply, energetically favorable ones. The sites contributing to primary metal oxidation will be on the ferrite laminae thereby giving rise to local roughening associated to surface area increments; this exposes new dissolution sites. Further, these precipitates that in time can cover most of the surface exposed to the electrolyte facing the microcells, lead to an increasing electrical resistance of the resulting electrochemical system coupled thereat; that is, provided they remain adhered to its parental surface.

When the electrolyte contains dissolved sulphates, the SO_4^{2-} anions may react with either, Fe(II) and with Fe(III) species forming solid species liable of precipitation, see Figure 1.

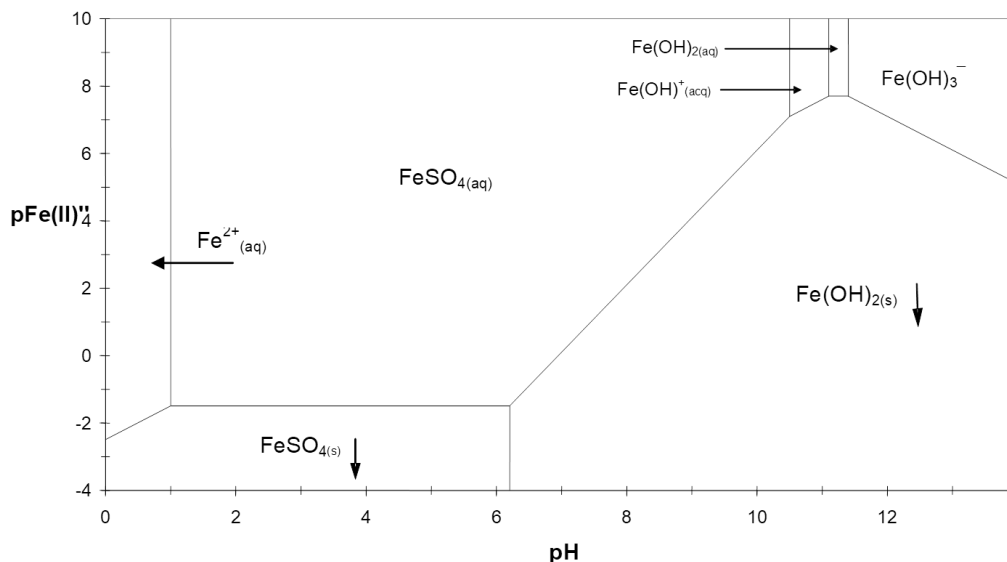


Figure 1. Predominance zones diagram for the system Fe(II) - SO₄²⁻ - H₂O - H⁺, constructed following Rojas-Hernández et al., methodology [8-11] and using the thermodynamic constants reported in [12], considering 1 M sulphate concentration.

In the case where the system is composed of Fe(III) - SO₄²⁻ - H₂O - H⁺ at the same sulphate concentration, the K_{ps} for Fe₂(SO₄)_{3(s)} is greater than that of FeSO_{4(s)}, which indicates that the former is more soluble, thus is incapable of forming a surface layer, possibly a passivating one. Therefore, the present work studies the formation of a passive layer composed of iron oxidation products formed on the surface of API 5L X52 samples, using cyclic voltammetry and chronoamperometry. The said methods will allow the analysis of the data generated during corrosion of the samples and the possible formation of a passivating layer through their nucleation and growth stages, to form an adherent surface layer.

2. EXPERIMENTAL DETAILS

2.1 API 5L X52 steel

Table 1 gives the nominal chemical composition of the steel used from the manufacturers' own specification sheet.

Table 1. Nominal chemical composition of the API 5L X52 steel. Chemical Composition (weight %)

Specification	Chemical Composition (weight %)													
	C	Mn	Si	P	S	Al	Nb	Cu	Cr	Ni	V	Ti	Ca	B
API 5L X52	0.08	1.06	0.26	0.019	0.003	0.039	0.041	0.018	0.02	0.019	0.054	0.003	0.0002	0.0003

The experiments were conducted on the steel prepared through conventional metallographic means, where the polyester resin-mounted samples had an exposed area of $\approx 0.83 \text{ cm}^2$ connected by a wire through the opposite side of the mount. Prior to each experiment the samples surfaces were ground and polished following conventional metallographic procedures, starting with 180 silicon carbide grit size and finishing with 1200 grit before polishing in napless cloth with alumina down to $0.3 \mu\text{m}$ and sonicated in deionized water subsequently followed by acetone.

2.2 Materials and instruments

The pH measurements of the solutions prepared with deionized water Type I ($18.2 \text{ M}\Omega\text{cm}$) were carried out with a Mettler Toledo pH-meter, with an error of ± 0.01 per pH unit. The electrochemical cell used was a typical three-electrode, with SCE as reference and a graphite bar as counter electrode. The potentiostat-galvanostat used was a EG&G Princeton 273 connected to a PC for control and data acquisition, through the Electrochemistry Power Suite software running. Exposure to the electrolyte was done keeping a minimum distance between the resin-mounted working electrode and the reference electrode to diminish the ensuing ohmic drop.

2.3 Solutions

The solutions used were as follows:

Solution 1: acid, $1 \text{ M H}_2\text{SO}_4$. (measured $\text{pH} = 0.11 \pm 0.01$)

Solution 2: neutral, $1 \text{ M H}_2\text{SO}_4$ and 2 M NaOH . (measured $\text{pH} = 6.99 \pm 0.02$)

Solution 3: basic, $1 \text{ M K}_2\text{SO}_4$ in a NaOH solution (measured $\text{pH} = 11.51 \pm 0.03$)

After exposure to the electrolytes, the samples were examined by means of a SEM instrument ESEM 30 XL Phillips fitted with EDS for chemical analysis as energy dispersive spectra obtained from the corrosion products.

3. RESULTS AND DISCUSSION

3.1 Voltammetry at different pH

Figure 2 shows the results obtained after linear sweep voltammetry assessment in each solution plotting current density, J , as a function of overpotential, η defined as the difference between the applied potential (E) and the open circuit potential (E_{ocp}) for the different pHs considered. It can be noted that passivation is very noticeable for pHs 6.99 ± 0.02 and 11.51 ± 0.03 , however, for $\text{pH} = 0.11 \pm 0.01$ the corrosion is active even for low overpotential values. This means that the anodic film formed at this pH ($\text{FeSO}_{4(s)}$, see Figure 1) promotes the corrosion process instead of inhibiting it, this result agrees with those reported by Bruzzoni and Garavaglia [1] regarding the increase in the hydrogen permeation through the iron oxide film formed in 0.1 N NaOH on the steel surface.

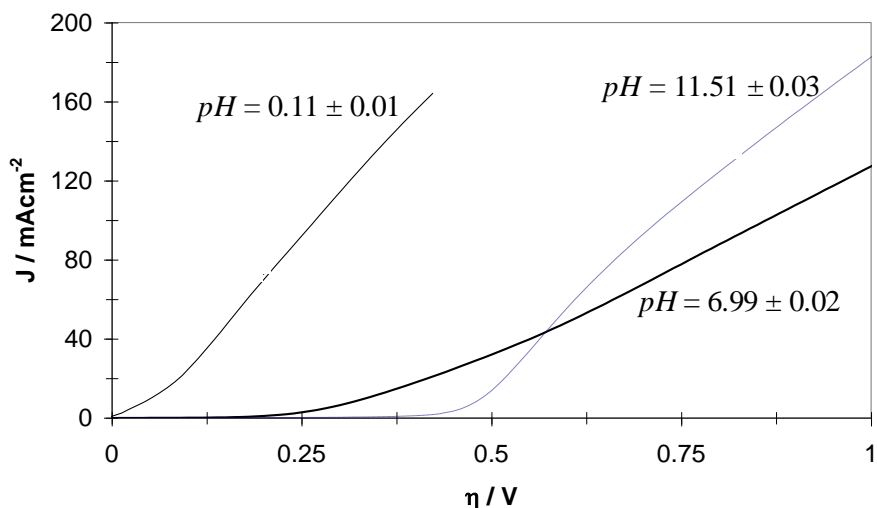


Figure 2. Current density variation as a function of the applied overpotential ($\eta = E - E_{ocp}$) obtained by linear sweep voltammetry at 0.1 mV/s in the system API 5L X52 in sulphate solution with different pH, as indicated in the figure.

3.2 Chronoamperometry at $pH = 0.11 \pm 0.01$

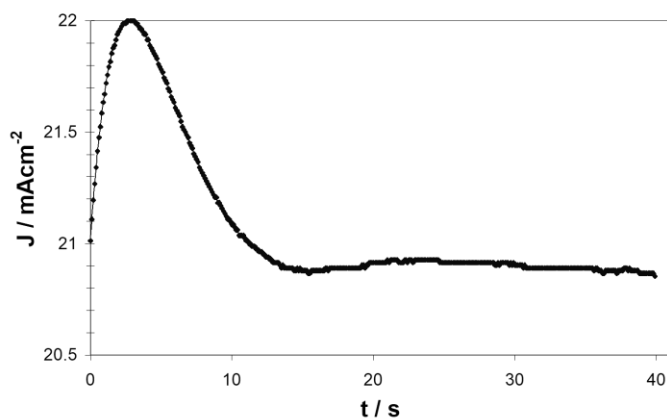


Figure 3. Chronoamperogram recorded in the system API 5L X52 / 1 M H₂SO₄ at $pH = 0.11 \pm 0.01$ at 500 mV overpotential.

Figure 3 shows a chronoamperogram obtained in the system API 5L X52 / 1 M H₂SO₄ at $pH = 0.11 \pm 0.01$; it depicts features corresponding with the electrochemical phase formation process of new a phase, FeSO_{4(s)}, on the electrode surface [2, 13-29]. See in particular references [2, 28-29] which are related with the anodic film formation of: PbSO_{4(s)} in lead-acid batteries [28], FeS_(s) during corrosion of steel in sour acid media [2] and FePO_{4(s)} during the electrochemical phosphatizing process of AISI-SAE steel samples, having different nominal carbon contents [29]. Note that at short times the oxidation rate increased rather rapidly for about 3 seconds and then decreased for another 12 s, thereafter the curve followed a constant trend.

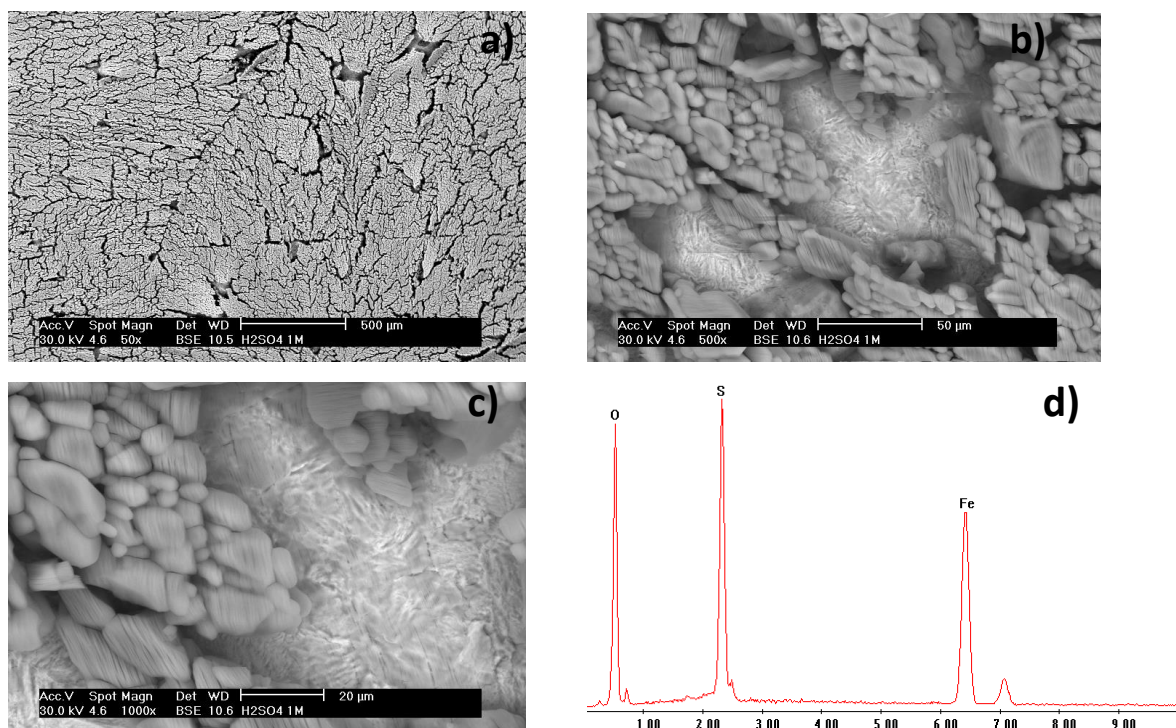


Figure 4. Secondary electron images of the API 5L X52 steel surface after the potentiostatic current transient shown in Figure 3 at different magnifications: **a) 50**, **b) 500**, **c) 1000X**. **d)** EDS spectrum taken at a point in the surface layer that covered the substrate, confirming the presence of the elements Fe, S and O.

Therefore, it becomes possible to suggest the formation of a passivating surface layer that was able to cover the steel surface within a relatively short 10 s period, however, as can be noted from the presence of a steady state current, the film formed does not passivate the corrosion process. Figure 4 a) shows a SEM micrograph of the working electrode surface after the chronoamperogram shown in Figure 3. Note the presence of a cracked layer comprising O, S and Fe revealed through EDS analysis, see Figure 4 b), which leads to assume that it may be formed by $\text{FeSO}_{4(s)}$. In contrast, the morphology and composition of the steel sample that was not exposed to the corrosive media is indeed different, see Figure 5. As a matter of interest, Yu *et al.* [4] reported potentiodynamic polarization and electrochemical impedance spectroscopy (EIS) of 15-5PH stainless steel that was measured in the 0.5 M Na_2SO_4 acid solution with various pH values and Cl^- concentrations. The authors found that at pH(1, 3, 5), the corrosion resistance of 15-5PH was enhanced, the corrosion current density (i_p) was reduced, and the passivity region increased. At pH 1, the hydrogen depolarization reaction was the main cathodic reduction process, with increasing pH value and that the passive film of 15-5PH stainless steel predominantly contained Cr-oxides, Ni-oxides, Fe-oxides and Cu species.

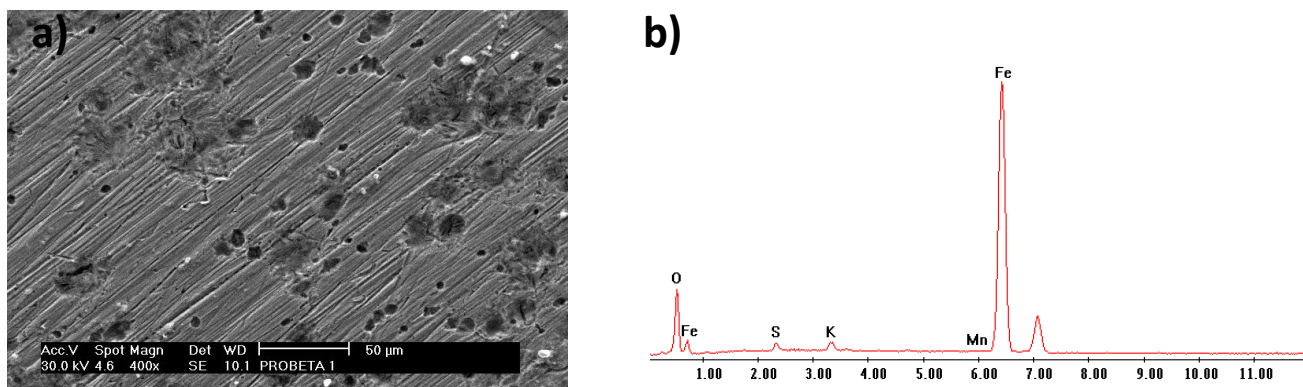


Figure 5. a) Secondary electron image of the API 5L X52 steel surface before the potentiostatic current transient shown in Figure 3 was applied, taken at **400X**. b) EDS spectrum taken at a point in the as-received-surface shown in a).

3.3 Chronoamperometry at $pH = 6.99 \pm 0.02$

Figure 6 shows chronoamperograms obtained in the system API 5L X52 / 1 M H₂SO₄ at $pH = 6.99 \pm 0.02$ applying different overpotentials, from which it becomes evident that the current at time $t = 0$ increases with increasing overpotential. There is not a sign of passivation taking place, although the corrosion rate stays constant with time.

After each experiment was carried out, it was noted the presence of some dark spots on the metal surface, although there was no formation of a continuous surface layer. In the cell, there appeared a greenish solute that changed colour as time passed to an orange hue, which suggests formation of iron (II) hydroxide or sulphate precipitate which did not adhere at all onto the metal surface, which explains why there was not a clear decrease of the current density.

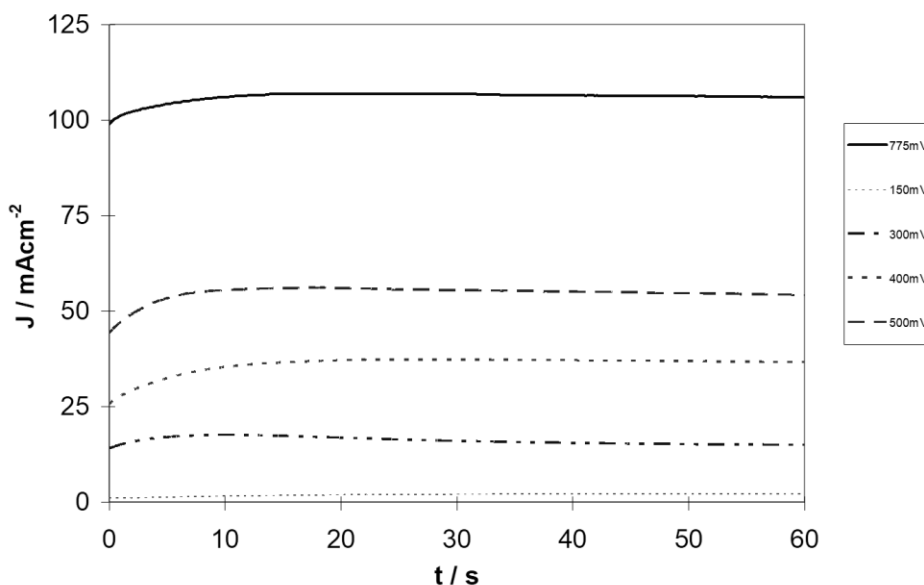


Figure 6. Chronoamperograms recorded in the system API 5L X52 / 1 M H₂SO₄ at $pH = 6.99 \pm 0.02$ for different applied overpotential indicated in the figure.

The remnant solution in the cell was drained and filtered: the powder collected was subsequently dried. Figure 7a) shows the general aspect of the powder with large and very small particles that may well have been crystals, and b) the EDS spectrum of the separated corrosion product, also confirming the hypothesis that the composition corresponded to an iron(II) sulphate-base salt, forming during the chronoamperometric pulse.

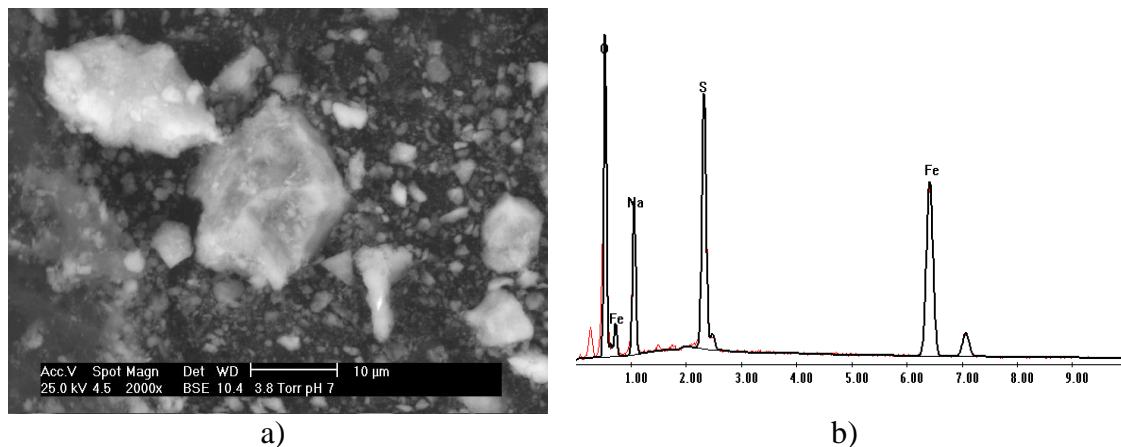


Figure 7. a) SEM micrograph obtained with secondary electrons at 2000X of the orange precipitate separated by filtration after the potentiostatic current transient shown in Figure 5 and b) its corresponding EDS spectrum.

3.4 Analysis of the corrosion products at $pH = 11.51 \pm 0.03$

The electrochemical characterization of the system API 5L X52 / K_2SO_4 1 M at $pH = 11.51 \pm 0.03$ showed that there was formation of a precipitate at the electrode surface, as in the previous case when the formation of a green precipitate was observed during voltammetry, that did not adhere onto the surface. The SEM image in Figure 8 a) shows that the surface film was not capable of full coverage, because the secondary electron image revealed more like islands, rather than a full-covering dark layer. This is thought to be the reason why the current density was not low enough, because the formation of the phase did not exhibit the same features as when full cover is achieved; therefore, this product cannot be considered as a passivating layer. The composition of the apparent crystals composing the islands corresponds to K_2SO_4 , probably formed after the sample dried out, which explains the presence of the peaks in the EDS spectrum shown in Figure 8 b), including the intense iron peaks from the substrate.

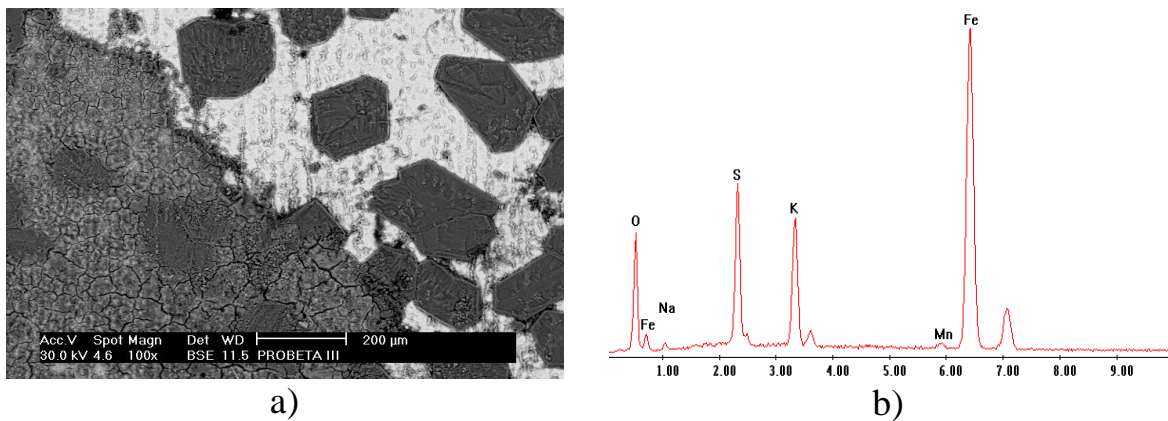


Figure 8. a) Secondary electron image at a 100X magnification of the electrode's surface after electrochemical testing in the system API 5L X52 / 1 M H₂SO₄ at pH = 11.51 ± 0.03. b) EDX spectrum obtained from the surface depicted.

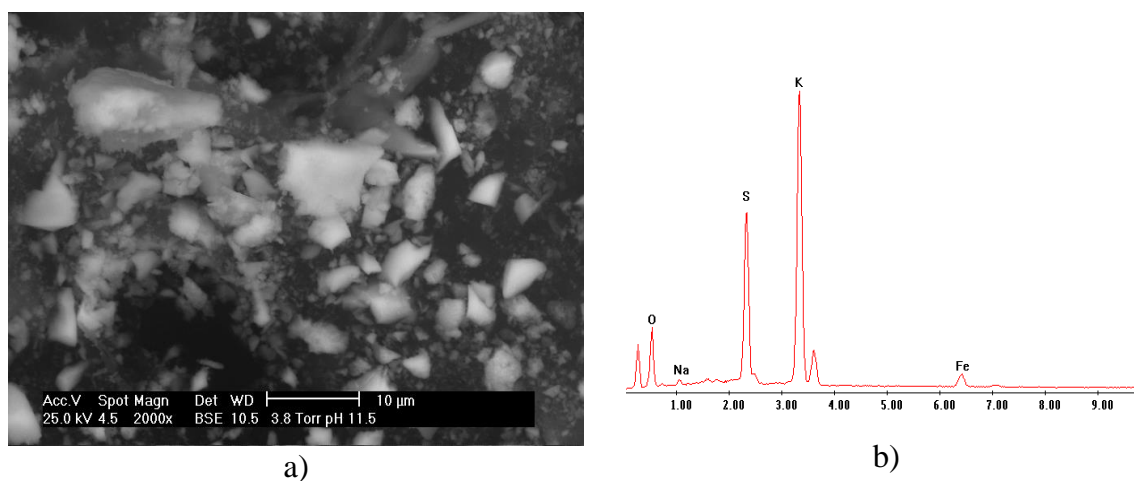


Figure 9. a) Secondary electron image at 2000X of the orange precipitate powder collected after filtration of the electrolytic solution of the system API 5L X52 / 1 M H₂SO₄ at pH = 11.51 ± 0.03. b) EDS spectrum showing the elemental composition of the reaction products that were collected as powder.

The oxidation product precipitates in the solution not adhering onto the metal surface. Just as before, the precipitate was filtered out and dried to be analyzed, and the powder collected is shown by the SEM image in Figure 9 a); the EDS spectrum shown in Figure 9 b), reveals once again, that the elements composing the corrosion product were: Fe, O and S, which can correspond to an iron-based sulphate. The presence of potassium, as in the previous case was due to crystallization of the remnant supersaturated electrolyte, containing K₂SO₄ as white crystals, onto the surface of the sample. Furthermore, similarly to the outcome of this work, the experimental study on alternating current corrosion of pipeline steel (X70) in alkaline environment by Yang *et al.* [5] concluded that the electrode surface is covered with a large amount of Fe(OH)_{ads}, when the potential was in the range of

the active dissolution potential of the X70 steel and that the hydroxide, as a corrosion inhibitor of the passive film, had an important impact on metal corrosion.

3.5 Influence of pH on the formation of corrosion products.

Figure 10 shows a comparison of the chronoamperograms obtained at the same overpotential and the different pH values. It can be noted that the oxidation current density at $\text{pH} = 6.99 \pm 0.02$ is slightly over twice that obtained at $\text{pH} = 0.11 \pm 0.01$ for the same time period, therefore, the oxidation rate at the latter pH was smaller as compared to that at $\text{pH} = 6.99 \pm 0.02$. This is related to the formation of the passive layer which managed to consolidate rather rapidly, namely after about 3 s, during immersion in the electrolyte, although it cracked afterwards. Conversely, as there was no formation of a layer that formed and covered the surface of the steel at neutral pH, passivation does not occur, although the oxidation rate attains a steady rate after a short period.

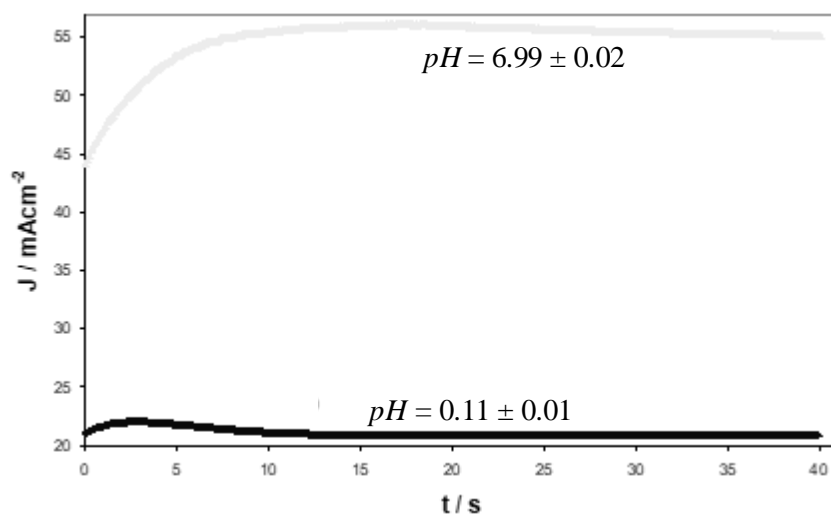


Figure 10. Comparison between chronoamperograms recorded at 500 mV overpotential in the system API 5L X52 in sulphate solution with different pH values indicated in the figure.

The formation of corrosion products on the steel surface was dependent on the solution pH change, that may produce a different effect; for instance, Flores-Frias *et al.* [6] studied the influence of pH on the use of *Salvia Hispanica* as green corrosion inhibitor for carbon steel in sulphuric acid and reported that this molecule acts as a good corrosion inhibitor however, it decreases with an increased solution pH.

4. CONCLUSIONS

The formation conditions of the surface layer formed electrochemically on the API 5L X52 steel were seen to depend clearly on the pH of the electrolyte, noting in particular the adhesion to the metal surface. From the thermodynamic analysis based on the predominance zones diagram used for

the system under study, a solid product was expected to form at $\text{pH} = 0.11 \pm 0.01$ though its physicochemical nature permitted to consolidate a surface reaction product which subsequently determined the course of the oxidation rate. The layer essentially proved to be formed by iron (II) sulphate. The same analysis indicated the possibility to form solid reaction products like the sulphate at $\text{pH} = 6.99 \pm 0.02$, and the hydroxide at $\text{pH} = 11.51 \pm 0.03$, but these were not adherent to the metal surface, although they could be recovered from the filtered out electrolyte after reaction.

ACKNOWLEDGEMENTS

M.R.R. and M.P.P. would like to thank CONACYT for project 22610714. M.R.R., M.T.R.S., M.G.M.Y. and M.P.P. gratefully acknowledge the SNI for the distinction of their membership and the stipend received. B.J. thanks the French government for the studentship that allowed his mobility period at México.

References

1. P. Bruzzoni, R. Garavaglia, *Corros. Sci.*, 33 (1992) 1797.
2. A. Hernández-Espejel, M.A. Domínguez-Crespo, R. Cabrera-Sierra, C. Rodríguez-Meneses, E.M. Arce-Estrada, *Corros. Sci.*, 52 (2010) 2258.
3. A. Hernández-Espejel, M. Palomar-Pardavé, R. Cabrera-Sierra, M. Romero-Romo, M.T. Ramírez-Silva, E. M. Arce-Estrada, *J. Phys. Chem. B*, 115 (2011) 1833.
4. Q. Yu, C.F. Dong, Z.B. Liu, J.X. Liang, K. Xiao, X.G Li, *Int. J. Electrochem. Sci.*, 10 (2015) 2035.
5. Y. Yang, S. Wang, C. Wen, *Int. J. Electrochem. Sci.*, 11 (2016) 7150.
6. E.A. Flores-Frias, J. Porcayo-Calderon, M.A. Lucio-Garcia, J.G. Gonzalez-Rodriguez, L. Martinez-Gomez, *Int. J. Electrochem. Sci.*, 12 (2017) 8227.
7. B. Li, Y. Huan, W. Zhang, *Int. J. Electrochem. Sci.*, 12 (2017) 10402.
8. A. Rojas-Hernández, M.T. Ramírez-Silva, J.G. Ibáñez, I. González, *J. Electrochem. Soc.*, 138 (1991) 365.
9. A. Rojas-Hernández, M.T. Ramírez-Silva, I. González, *Anal. Chim. Acta*, 278 (1993) 321.
10. A. Rojas-Hernández, M.T. Ramírez-Silva, I. González, *Anal. Chim. Acta*, 278 (1993) 335.
11. A. Rojas-Hernández, M.T. Ramírez-Silva, I. González, *J. Chem. Ed.*, 72 (1995) 1099.
12. C. Baes, R. Mesmer (1986), 'The Hydrolysis of Cations', 2nd ed. Robert E. Krieger, Publishing, Malabar, FA, p.211.
13. M. Palomar-Pardavé, I. González, N. Batina, *J. Phys. Chem. B*, 104 (2000) 3545.
14. B. R. Scharifker, J. Mostany, M. Palomar-Pardavé, I. González, *J. Electrochem. Soc.*, 146 (1999) 1005.
15. M. Palomar-Pardavé, B.R. Scharifker, E.M. Arce, M. Romero-Romo, *Electrochim. Acta*, 50 (2005) 4736.
16. E. Barrera, M. Palomar-Pardavé, N. Batina, I. González, *J. Electrochem. Soc.*, 147 (2000) 1787.
17. A. Serruya, B. R. Scharifker, I. González, M.T. Oropeza, M. Palomar-Pardavé. *J. Appl. Electrochem.*, 6 (1996) 451.
18. M. Palomar-Pardavé, M.T. Ramírez, I. González, A Serruya, B.R. Scharifker. *J. Electrochem. Soc.*, 143 (1996) 1539.
19. A.B. Soto, E.M. Arce, M. Palomar-Pardavé, I. González. *Electrochim. Acta*, 41 (1996) 2647.
20. M. Miranda-Hernández, M. Palomar-Pardavé, I. González, N. Batina. *J. Electroanal. Chem.*, 443 (1998) 81.
21. M. Palomar-Pardavé, I. González, A.B. Soto, E.M. Arce. *J. Electroanal. Chem.* 443 (1998) 125.

22. M. Palomar-Pardavé, M. Miranda-Hernández, I. González, N. Batina. *Surf. Sci.* 399 (1998) 80.
23. M. Palomar-Pardavé, M. Miranda-Hernández, I. González, N. Batina. In *Fundamental Aspects of the Electrochemical Deposition and Dissolution Including Modeling*, M. Paunovic, M. Datta, M. Matloss, T. Osaka and J. B. Talbot, Editors, PV 97-27, Paris-France-September 1997, ISBN-1-56677-180-3, pp. 27-40.
24. M. Palomar-Pardavé, M. Miranda-Hernández, N. Batina, I. González. In *Recent Research Developements in Electrochemistry*" S.G. Pandalai, (Editor). Transworld Research Network, Trivandrum, India. 1 (1998)15-29. ISBN-81-86846-18-2.
25. L. H. Mendoza-Huizar J. Robles, M. Palomar-Pardavé. *J. Electroanal. Chem.* 521 (2002) 95.
26. M. Palomar-Pardavé, I. González, N. Batina. *J. Phy. Chem. B.* 104 (2000) 3545.
27. L. H. Mendoza-Huizar J. Robles, M. Palomar-Pardavé. *J. Electroanal. Chem.* 545 (2003) 39.
28. L.I. Espinoza-Ramos, J. M. Hallen-López, C. Ramírez, E. Arce, M. Palomar-Pardavé, M. Romero-Romo. *J. Electrochem. Soc.* 149 (2002) B543.
29. M. Palomar-Pardavé, M.T. Ramírez-Silva, G.A. Vázquez-Coutiño, M. Romero-Romo, H. Herrera-Hernández, M. G. Montes de Oca-Yemha. *J. Solid State Electrochem* 17 (2013) 459.

© 2018 The Authors. Published by ESG (www.electrochemsci.org). This article is an open access article distributed under the terms and conditions of the Creative Commons Attribution license (<http://creativecommons.org/licenses/by/4.0/>).